Invited Paper

Terahertz photoconductive antenna with all-dielectric nanopillars

Kemeng Wang [1], Jianqiang Gu [1*], Wenqiao Shi [1], Youwen An [1] and Weili Zhang [2]
[1] Center for Terahertz Waves and College of Precision Instrument and Optoelectronics Engineering, Tianjin University, Tianjin 300072, China
[2] School of Electrical and Computer Engineering, Oklahoma State University, Stillwater, OK 74078
[*1] Email: gjq@tju.edu.cn

(Received 28 September 2020)

Abstract: Photoconductive antennas (PCAs), as a popular terahertz (THz) radiation source, have been widely used in spectroscopy, material characterization, biological imaging and detection of hazardous materials. However, PCAs have a relatively low energy conversion efficiency from femtosecond laser pulses to THz radiation which often limits the signal-to-noise ratio and bandwidth of THz imaging and spectroscopy systems. To address these limitations, here we report a THz photoconductive antenna emitter with all-dielectric nanopillars integrated on top of the SI-GaAs substrate to increase the generated photocarriers, which achieves a broadband and frequency insensitive THz power enhancement factor around 1.25 at frequencies 0.05 - 1.6 *THz*. Our results reported here provide a new method for increasing the THz power of PCAs, which paves the way for the subsequent researches of next-generation PCAs.

Keywords: Terahertz, Nanopillars, Photoconductive antenna, All-dielectric metamaterials

doi:

1. Introduction

Photoconductive antennas (PCAs) have always been widely used by the research community because of number of advantages, such as compact in size, low cost, fiber technology compatible and room temperature operation. However, the radiated THz power of PCAs is at a level that does not meet the rapidly growing demand in the field of THz science and technology. Improving THz efficiency of PCAs has always been a challenging task [1-7]. To address this problem, the O'Hara firstly integrated a split ring resonator into the electrodes of a PCA transmitter [8]. Subsequently, several groups have attempted to carry forward this method through implementation of metallic nanostructures which locally enhance the interaction between the femtosecond laser pulse and the semiconductor substrate of the PCAs [9-14]. The improved emission behavior of these metamaterial assisted PCAs arouses enormous interests in the THz research. However, metallic nanostructures also suffer from Ohmic loss and poor heat resistance. Dielectric nanostructures, on the other hand, having neglectable Ohmic loss and good heat resistance, began to attract attention from researchers: Khorshidi M. and his co-workers theoretically analyzed a dielectric structure for increasing radiation power of PCA [15]; Rana, G. et al. reported a PCA with an array of hexagonal holes for enhanced THz emission, which discussed the polarization dependence of the dielectric nano-hole array on the optical pump [16];

recently, we have achieved a significant PCA power enhancement through etching nanogratings directly on the surface of the PCA substrate [17]. The integrated nanopillars not only maximizes the generation of photocarriers, but also benefits the bias electric field loaded on the photocarriers. Besides PCA emitters, recently two sorts of dielectric nanostructures were also introduced to enhance the sensitivity of a THz PCA detector [18, 19].

In this letter, we propose and demonstrate a dielectric nanopillars assisted PCA transmitter having a nearly uniform THz power enhancement factor in a broad bandwidth. We optimize the performance of PCAs by improving the optical absorption and obtained nearly consistent THz enhancement. As we present in ref. 17, the optical absorption improvement is due to the multiple beam inference instead of Mie or plasmonic resonances, which permits to fabricate the nanopillars by dry etching the substrate itself, preventing the complex dielectric layer growth process and the unknown metal-semiconductor contact problems encountered in previous nano-structure assisted PCAs.

2. Concept and design

The PCA with all-dielectric nanopillars (NP-PCA) is schematically shown in Figure 1(a). The PCA is comprised of a semi-insulating gallium arsenide (SI-GaAs) substrate of a thickness of $350\mu m$ and a pair of coplanar transmission lines separated by 80 μm. The width of the coplanar transmission line is 20 μm. The 50×80 μm^2 nanopillar array is etched on the top of the substrate and near the anode transmission line. A silicon lens is attached at the backside of the substrate to collect the emitted THz radiation (not shown in the Figure 1(a)). We carried out numerical studies on the interaction between the nanopillars and the incident pump light, where the duty ratio and the height of the nanopillar were scanned to minimize the reflectivity of optical pump in the time-domain solver of CST Microwave Studio.

In order to compare the radiation characteristics of PCAs with nanopillars designed for different wavelengths, nanopillar arrays with varying widths (w~160, 170, 185, 200, 210, 215, and 230 *nm*) were fabricated along the inner side of the same anode as Figure. 1(b) shows. As shown in Figure. 1(c), the fabrication of NP-PCA is in two steps: the nanopillar array etching and photolithography fabrication of PCA. The nanopillar array was fabricated on a 350-μm-thick semi-insulating gallium arsenide wafer. Firstly, a layer of positive electron beam resist with a thickness of 430 *nm* was spin-coated on the substrate, followed by baking for 2 *min* at 180°. Then the patterned resist mask was generated by E-beam lithography. The sample was then successively developed in the solution of n-amyl acetate containing 0.45% butanone and in isopropyl alcohol. Next, the nanostructures were formed by ICP etching. Finally, the residual electron beam resist was removed by butanone and isopropyl alcohol. In the second step, the wafer with the nanostructures was spin-coated by a layer of positive photoresist S1813 with a thickness of 1.5 μm, followed by baking for 1 min at 115°. Then the PCA pattern was transferred

by conventional photolithography under the precise alignment with the nanostructures, then baked for 20 s at 115°. After baking, the sample was developed in TMAH 2.38% then baked for 15 s at 115°. Next, the residual resist was removed by O_2 plasma. Finally, the PCA's coplanar transmission lines were thermal evaporation deposited with Ti/Au (10 *nm*/200 *nm*), and the residual photoresist was removed by acetone. One completed NP-PCA was assembled onto a specifically designed PCB board which has SMA connectors to apply the bias voltage. Each array has the same area of 50×80 μm^2, and is separated 150 μm away from others, as shown in Fig. 1(b), these PCAs were numbered from NP-PCA1 to NP-PCA7 in a sequence. For more accurate comparison of NP-PCAs and their corresponding references which are 75 μm away from the adjacent nanopillar array along the transmission line direction, we choose the averaged results of the two positions adjacent of NP-PCA as the references of NP-PCA. In this way, we minimize the influence of the reference position along the transmission line.

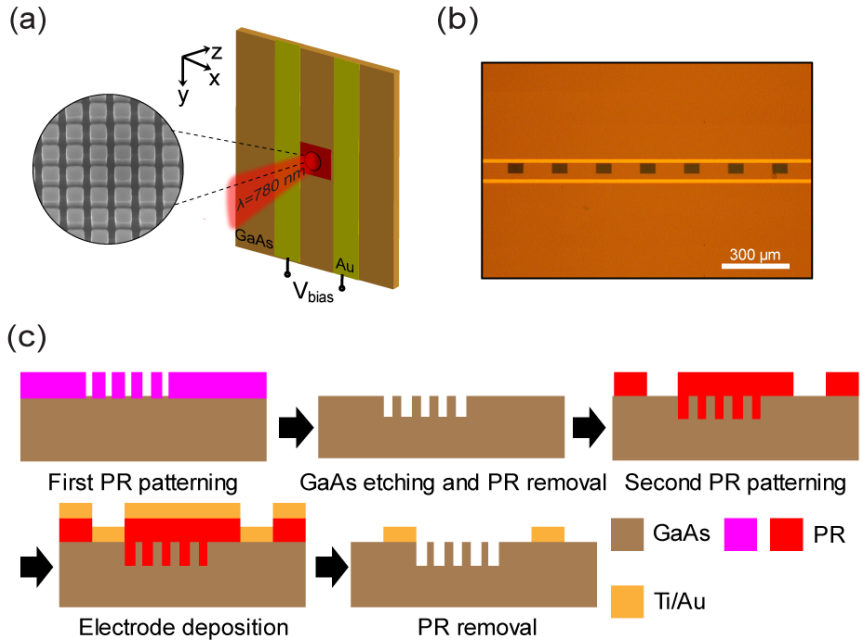

Fig. 1 Design and fabrication of NP-PCAs. (a) Schematic diagram of the NP-PCA. The circular image is a partial magnification of the nanopillars, the period of the unit cell: p = 350 *nm*, the height of the unit cell: h = 230 *nm*. (b) Microscopy photo of the fabricated PCA with the nanopillar arrays. (c) Hierarchical fabrication procedure for the NP-PCAs with SI-GaAs nanopillars. PR: photoresist. The purple color of PR is positive electron beam resist and the red color of PR is positive photoresist S1813.

3. Characteristics of NP-PCAs

The optical reflectance of the nanopillar arrays and the bare substrate were measured in a home-built reflectance test setup as Figure 2(a) shows, in which a lamp (wavelength range: 360–2600 *nm*) was used to generate broadband illuminance. The lens L1 focuses the incident light from the lamp onto the antenna sample and the reflected light is collected and collimated by

the lens L1. The reflected light from the nanopillars is collected by the fiber detector of a spectrometer (wavelength range: 200-1100 *nm*). In order to align the nanopillars to the focus of the incident light, a reflective microscopic optics was also added. The green light emitted by a laser diode (LD) is introduced into the optics through a thin film beam splitter BP1 and adjusted to be coaxial with the broadband light from the lamp. The green light then propagates as the broadband light does until it is separated out of the system by another thin film beam splitter BP3. Then the reflected image of the sample is collected by a CCD. As shown in Figures 2(b) and 2(c), this microscopy imaging system can clearly observe the antenna, the nanopillars and the broadband light focus, which clearly present a drastically reduced pump reflectance. The optical reflectance ratio was calculated by the following formula: $R_s(\lambda)=(S(\lambda)-B(\lambda))/(R(\lambda)-B(\lambda))\times 100\%$, where $S(\lambda)$ and $R(\lambda)$ represent the reflected light of the nanopillars and the bare substrate, respectively, and $B(\lambda)$ is the background signal of the setup. The detailed reflectance measured by spectrometer is shown in Figure 2(e). The reflectance minimal wavelength varies with the width of the nanopillars, which is in good agreement with the evaluation according to the multiple beam interference as well as the simulation results (Fig. 2(d)). The proposed nanopillars have a lowest reflectance (~7.53%) around 780 *nm* when w = 215 *nm*, which means that nearly 1.4 times more photocarriers should be generated than the bare SI-GaAs substrate.

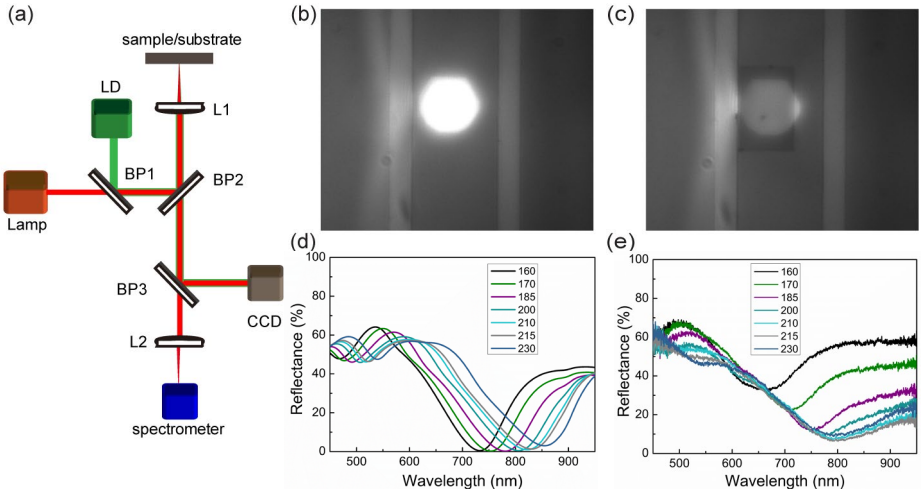

Fig. 2 Reflectance characteristics of nanopillars with varying widths. (a) Experimental setup for the reflectance measurement. BP: beam splitter, L: lens. CCD images of (b) the substrate and (c) the nanopillars illuminated by wideband light source, respectively. (d) Numerically evaluated reflectance of the nanopillars. (e) Experiment results of the reflectance for the nanopillars, the lowest reflectance of the pump beam is ~7.53% when w = 215 *nm* around the wavelength of 780 *nm*.

The THz radiation characteristics of NP-PCAs were investigated in a 4F THz time-domain spectroscopy system (see Ref. 17 for details about the system), where the electric field of THz pulses from the NP-PCAs and the references were recorded at 15 *V* bias voltage and 6 *mW* laser excitation power. Figure 3 presents the measured results for NP-PCA6, which shows the clearest enhancement effect among the seven nanopillar arrays. As can be seen in the time domain

(Figures 3(a)), the NP-PCAs' amplitudes are larger than the references. The Fourier transform also reveals this enhancement, as shown in Figure 3(b), the NP-PCA6 have higher amplitude over the whole bandwidth than the references, from 0.05 to 1.6 *THz*. Considering the only difference between the NP-PCA and the references is the nanopillar array, it is reliable to conclude that this enhancement is contributed to the anti-reflection function of the nanopillars, which enables more photocarriers in the substrate, thus leading to a higher THz emission. In addition, it is interesting to find that the enhancement factor of each NP-PCA is nearly unchanged from 0.05 - 1.6 *THz*, which is around 1.25 for NP-PCA6. This frequency insensitive characteristic is also identically embodied in the time domain, in which the shape and delay of the THz pulses of the NP-PCAs are nearly the same as those of the references. This property, which is essential for next generation PCA design, is a distinguishing feature of our PCA from previous designs [9-14].

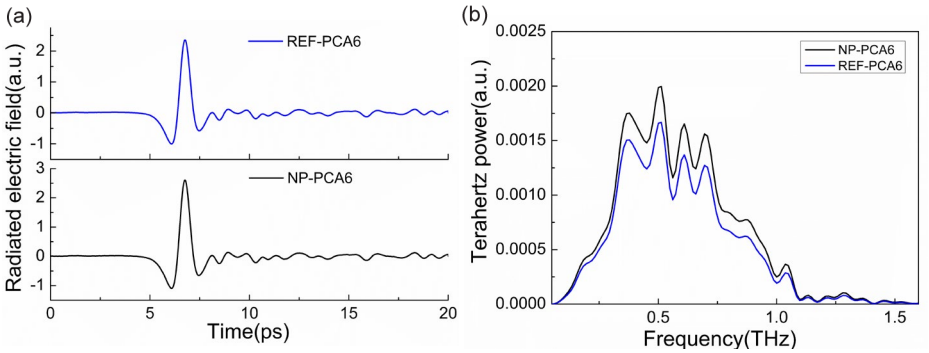

Fig. 3 Comparison of NP-PCAs and REF-PCAs. (a) THz electric field in the time domain of NP-PCA6 (black line) (w = 215 *nm*) and REF-PCA6 (blue line). (b) THz power spectra from NP-PCA6 (black line) and REF-PCA6 (blue line).

Combined with the reflectance measurement (Figure 2e), it is easy to understand why NP-PCA6 that shows lower reflectance (~7.53%) around 780 *nm* presents the highest THz enhancement. However, it is noticed that the reflectance variation of the nanopillar arrays cannot explain all the NP-PCAs' behavior, as shown in Figure 4. Specifically, the THz enhancement of NP-PCA3 and NP-PCA4 violates the proportional law with the reflectance. Even more confusing, NP-PCA1, NP-PCA2 and NP-PCA7 show negative or tiny enhancement compared to their references, despite that all nanopillar arrays increase the absorption of the optical pump more or less. According to our previous studies reported in ref. 17, the enhancement of THz radiation caused by the nano-structures not only depends on the reduced reflection of the laser illuminance, but also relates to the changed bias electric field altered by the nano-structures. Thus, the unexpected behavior of NP-PCA1, NP-PCA2, NP-PCA4 and NP-PCA7 may due to the fabrication errors and/or the influence of the nanopillars on the bias electric fields.

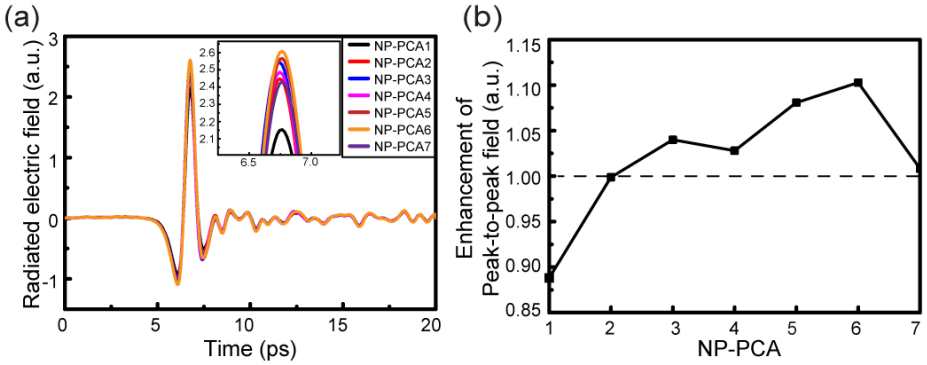

Fig. 4 THz radiation characteristics of NP-PCAs with varying width nanopillars. (a) Radiated THz electric field in the time domain of NP-PCAs with varying width nanopillars. (b) Enhancement of peak to peak values of the radiated electric field between the seven NP-PCAs and their corresponding references.

4. Conclusions

In summary, we demonstrated a category of dielectric nanopillars to improve THz generation efficiency of PCAs by lowering the reflectance of the pump laser pulse. With this approach, we experimentally achieved a sharply reduced reflectance for the pump laser pulses (λ = 780 *nm*). Thus, an outstanding PCA with an average terahertz power enhancement factor of 1.25 at frequencies 0.05 - 1.6 *THz* was obtained. We believe that our results may pave a way toward developing next generation of THz PCA emitters.

References

[1] D. H. Auston, K. P. Cheung, and P. R. Smith. “Picosecond photoconducting Hertzian dipoles”. *Appl. Phys. Lett*. 45, 284-286 (1984).

[2] S. Preu, G. H. Dohler, S. Malzer. et al. “Tunable, continuous-wave terahertz photomixer sources and applications”. *J. Appl. Phys.* 109, 061301 (2011).

[3] S. Matsuura, M. Tani, and K. Sakai. “Generation of coherent terahertz radiation by photomixing in dipole photoconductive antennas”. *Appl. Phys. Lett.* 70, 559-561 (1997).

[4] A. Nahata, A. S. Weling, and T. F. Heinz. “A wideband coherent terahertz spectroscopy system using optical rectification and electro-optic sampling”. *Appl. Phys. Lett.* 69, 2321-2323 (1996).

[5] M. B. Ketchen. “Generation of subpicosecond electrical pulses on coplanar transmission lines”. *Appl. Phys. Lett.* 48, 751-753 (1986).

[6] P. U. Jepsen, R. H. Jacobsen, and S. R. Keiding. “Generation and detection of terahertz pulses from biased semiconductor antennas”. *JOSA B*. 13, 2424-2436 (1996).

[7] M. Van Exter, and D. R. Grischkowsky. “Characterization of an optoelectronic terahertz beam system”. *IEEE T. Micro. Theory*. 38, 1684-1691 (1990).

[8] J. F. O'Hara, H. Chen, A. J. Taylor, et al. "Split-Ring Resonator Enhanced Terahertz Antenna". *Nonlinear Optics: Materials, Fundamentals and Applications, Optical Society of America.* TuB2 (2007).

[9] S. G. Park, et al. "Enhancement of terahertz pulse emission by optical nanoantenna". *ACS Nano*. 6, 2026 -2031(2012).

[10] A. Jooshesh, et al. "Nanoplasmonics enhanced terahertz sources". *Opt. Express*. 22, 27992-28001 (2014).

[11] C. W. Berry, N. Wang, M. R. Hashemi, et al. "Significant performance enhancement in photoconductive terahertz optoelectronics by incorporating plasmonic contact electrodes". *Nat. Commun.* 4, 1622 (2013).

[12] M. Bashirpour, M. Forouzmehr, S. E. Hosseininejad. et al. "Improvement of terahertz photoconductive Antenna using optical Antenna Array of ZnO Nanorods". *Sci. Rep.* 9, 1414 (2019).

[13] S. Lepeshov, et al. "Boosting terahertz photoconductive antenna performance with optimised plasmonic nanostructures". *Sci. Rep.* 8, 6624 (2018).

[14] N. M. Burford, M. J. Evans and M. O. El-Shenawee. "Plasmonic Nanodisk Thin-Film Terahertz Photoconductive Antenna". *IEEE T. THz Sci. Techn.* 8, 237-247 (2017).

[15] M. Khorshidi and G. Dadashzadeh. "Dielectric structure with periodic strips for increasing radiation power of photoconductive antennas: theoretical analysis". *J. Infrared, Millim., Terahertz Waves.* 38, 609-629 (2017).

[16] G. Rana, et al. "A Polarization-Resolved Study of Nanopatterned Photoconductive Antenna for Enhanced Terahertz Emission". *IEEE T. THz Sci. Techn*. 9, 193-199 (2019).

[17] Kemeng Wang, Jianqiang Gu, Wenqiao Shi, et al. "All-dielectric nanograting for increasing terahertz radiation power of photoconductive antennas". *Optics Express*. 28(13):19144-19151(2020).

[18] O. Mitrofanov, et al. "Efficient photoconductive terahertz detector with all-dielectric optical metasurface". *APL Photonics.* 3, 051703 (2018).

[19] T. Siday, et al. "Terahertz Detection with Perfectly-Absorbing Photoconductive Metasurface". *Nano Letters.* 19, 2888-2896 (2019).